Final Technical Report

NEHRP/USGS Award Number: G15AP00003 and G15AP00004

Does consideration of fault interaction improve the predictability of repeating earthquake sequences at Parkfield?: Collaborative Research with University of California, Berkeley, and Indiana University

Robert M. Nadeau
Berkeley Seismological Laboratory and
Berkeley Institute of Data Science
University of California, Berkeley
215 McCone Hall
Berkeley, CA 94720-4767
Telephone: 510-643-3980; Fax: (510) 643-5811
Email: nadeau@seismo.berkeley.edu

Prof. Roland Bürgmann
Berkeley Seismological Laboratory and
Dept. of Earth and Planetary Science
University of California, Berkeley
307 McCone Hall
Berkeley, CA 94720-4767
Telephone: 510-643-9545; Fax: 510 643-9980
Email: burgmann@seismo.berkeley.edu

Prof. Kaj Johnson
Dept. of Geological Sciences
Indiana University
GY401
1001 East 10th Street,
Bloomington, IN 47405-1405
Telephone: 812-855-3612; Fax: 812-855-7899
Email: skajjohns@indiana.edu

Prof. Kate Huihsuan Chen
Dept. of Earth Sciences
National Taiwan Normal University
No. 88, Sec. 4, Tingzhou Rd.,
Wenshan District, Taipei, Taiwan 11677
Telephone: +886-2-77346400; Fax: +886-2-2933-3315
Email: katepili@gmail.com

Term covered by this award: December 1, 2014 – November 30, 2015

ABSTRACT:

The study of what governs the timing of characteristic earthquakes is a key to understanding the nature of the earthquake cycle and to determining earthquake hazard, yet the control of the recurrences is not well established. Statistical models for estimation of earthquake probabilities employ mathematical distributions that are thought to properly represent stochastic properties of earthquake recurrence. Many factors may contribute to the irregularity of earthquake recurrence and variability in earthquake magnitude, such as inherent heterogeneity of stress, strength and slip on a fault, temporal and spatial variations in fault healing, and variability in the evolution of fluid pressure. Fault interaction, in the form of advances or delays in earthquake recurrence from changes in the stress field by nearby earthquakes and their postseismic deformation transients, is also believed to play a first-order role in this behavior. Numerous studies suggest importance of fault interaction in the distribution of aftershocks and the development of earthquake sequences. However, much debate continues about the relative importance of static and dynamic stresses in earthquake triggering and the stress magnitude required to produce significant triggering. Most importantly, the lack of observational documentation of the statistical significance of such interaction in natural earthquake populations has limited the utility and use of fault interaction modeling in formal earthquake probability estimates.

In this project, we build on more than a decade of work establishing a record of repeating micro-earthquakes with data from the borehole HRSN network and surface NCSN network sites at Parkfield, CA. By the end of 2015, 217 repeating-earthquake sequences ranging from M = -0.4 to M = 3 with up to 83 recurrences of near-identical ruptures of isolated asperities were identified within this partly creeping transition segment of the San Andreas fault (SAF). We used this large earthquake population to examine, model and test if fault interaction in the form of static stress changes and transient postseismic fault creep produces much of the observed aperiodicity in the occurrence of these events. Using the large number, precisely known locations, and frequent repeats of these events, we (1) examined the catalog for empirical evidence of earthquake triggering and event sequences and (2) explicitly modeled the mechanics of such interaction. This has allowed us to evaluate the role of fault-interaction stresses in the timing of observed event sequences. We worked to separate the effect of changes in recurrence intervals that stem from documented coherent accelerations of fault slip, such as have been observed in the mid-1990s and following the 2004 Parkfield earthquake, from those caused by local interactions. We developed physical models of the slip events and afterslip on the surrounding SAF and their interactions building on existing boundary element methods that allow for consideration of time-dependent stress changes. And we explicitly considered the role of the 2004 earthquake in the spatio-temporal development of the repeating earthquake sequences. Using the models, we have also venture to explicitly examine if fault interaction

through stress transfer determines recurrence history and aperiodicity of earthquakes among sub-populations of the Parkfield repeating earthquakes.

To aid in the interpretation of the mechanical modeling, we also participated in finite-source inversion efforts of the SF (San Francisco) M2 repeating earthquake sequence from the San Andreas Fault Observatory at Depth (SAFOD) experiment. This effort has given us a better understanding of the role of heterogeneity in earthquake slip and how such heterogeneity may affect our stress modeling results. We also participated a complementary study on a larger scale relating transient seismicity to episodes of deep creep from repeating earthquakes and non-volcanic tremor, Coulomb stress transfer and the 2004 Parkfield M6 mainshock. These efforts directly address priorities in the Earthquake Physics and Occurrence program that may improve implementation of fault interaction physics in the development of time dependent earthquake probability estimates.

REPORT:

A. Modeling Repeating Earthquake Interactions: Triggering effect from nearby microseismicity

1. Introduction

The large population of repeating micro-earthquakes at Parkfield provides a unique opportunity to examine, model and test the extent to which fault interaction in the form of static stress changes and transient postseismic fault creep produces changes in frequency and magnitude of the events. Our earlier efforts in *Chen et al.* [2013] selected a subset of 112 double-difference relocated [*Thurber et al.*, 2006], M 0.4 ~ 3.0 sequences to examine the interactions and triggering effect from nearby microseismicity. Taking advantage of the large number of repeating microearthquakes with precisely determined relative locations, we analyzed the repeating-event catalog for empirical evidence of interaction.

Chen et al. [2013] documented strong evidence for short-term triggering by nearby earthquakes either by static or dynamic stressing (Fig. 1), but failed to find evidence for a strong correlation between the static stress changes an RES asperity experiences prior to its next event and the length of the corresponding recurrence interval (Fig. 2a). Short-term triggering is reflected in the increased rate of events, and especially of events producing (incurring) higher stress changes during the days preceding (following) an RES event (Fig. 1). Stress changes computed in the "postshock" case are those imposed by the RES on the subsequent events, whereas in the "preshock" case the stress changes are those imposed on the RES event. They found that the rates of nearby preshocks and postshocks systematically increase with decreasing time before and after an RES event and this increase is most pronounced for events that imposed or experienced higher stress changes. As the time difference between RES and background events (DT) gets shorter the relative contribution of very high

stress-change events increases. When considering the > 1 kPa events, 73% of preshocks occurring within $|DT| < 1$ day are found to have a greater magnitude than the following RES events; i.e., the repeaters can be considered aftershocks. The population of RES that experienced stress change rate greater than 1 MPa/yr is also found to have a mean normalized recurrence interval of 0.89 (median value = 0.86) (Fig. 2). This suggests that a modest but significant reduction of recurrence intervals is taking place when estimated average stressing rates due to neighboring earthquakes during a recurrence interval exceed 1 MPa per year.

However, in *Chen et al.* [2013] the computation of stress change from all nearby RESs and background events relied on a simple expression for the static shear stress change $\Delta\sigma = 1/6\ \pi\ \mathrm{Mo}/r^3$ [*Aki and Richards*, 1980], where r is the distance from a RES to the hypocenter of each neighboring event (with seismic moment Mo). Empirical tests using the shear stress change calculated from an elastic dislocation model [*Okada*, 1992] produce consistent values of in-plane stress changes. In these calculations we assumed that all earthquakes lie on a single plane and thus increase stress on their neighbors, which is clearly not always the case due to geometric complexity of the active fault strands. In addition, the aseismic slip derived stress change is neglected in the computation using the *Aki and Richards* [1980] expression (referred as A&R relation hereafter). To better understand how the stress interaction controls the RES's recurrence interval and timing, it is important to have a more accurate stress model focusing on important effects of 3D geometry and aseismic fault creep.

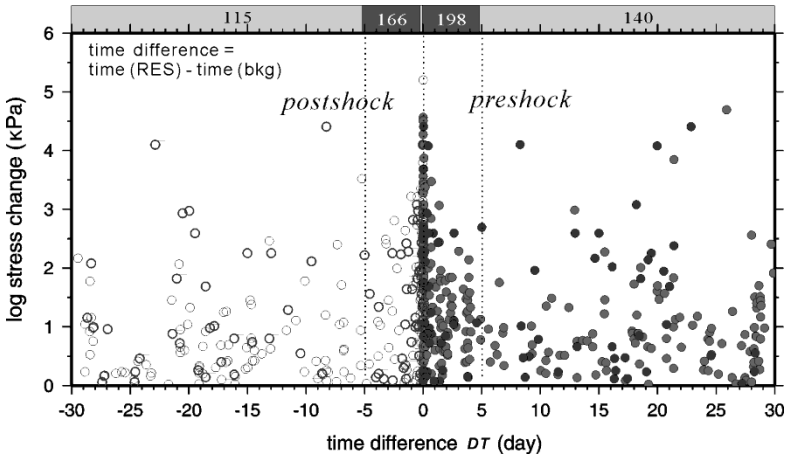

Figure 1. Static stress change as a function of time difference between repeating events and background earthquakes (bkg) within one month and 5-km distance (only events with stress changes > 1 kPa are shown). Top labels indicate the number of nearby events with stress changes > 1 kPa within 5 days and 5-30 days following/preceding the RES events (from *Chen et al.*, 2013).

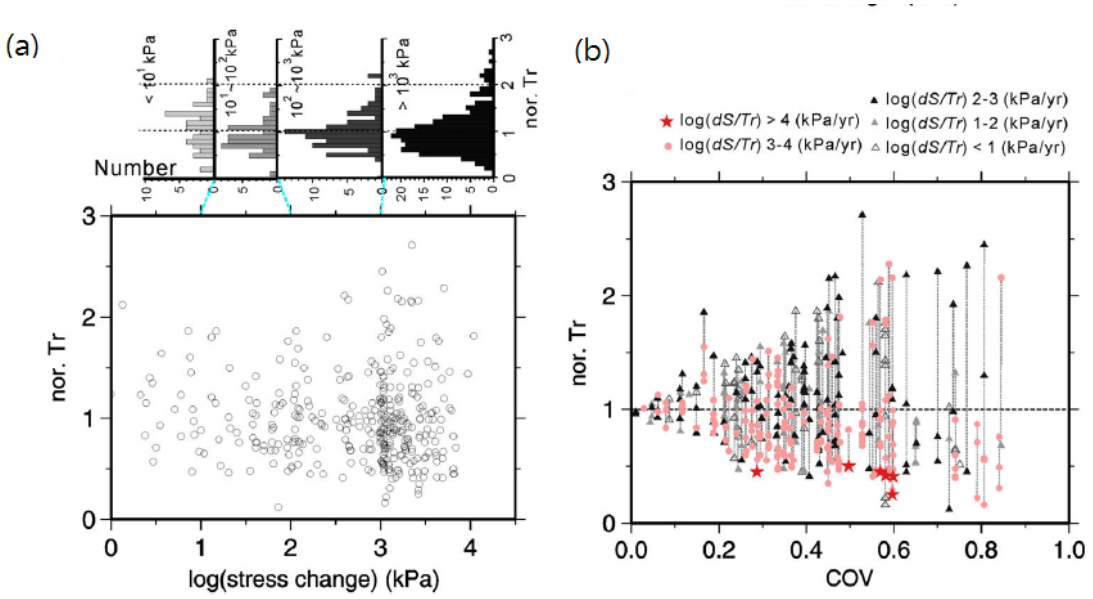

Figure 2. (a) (Lower panel) Normalized recurrence interval (Tr) of all RES events as a function of stress change during the preceding recurrence interval. (Upper panel) Histograms of normalized recurrence intervals for different stress change ranges. (b) Normalized Tr values as a function of COV of each RES. The RES events exposed to different ranges of stressing rate are indicated by different symbols. Vertical dashed line connects the data points belonging to the same sequence.

2. Methods

Based on our knowledge of the fault geometry, location of events, and distribution of aseismic creep, we develop rate-state friction boundary element models that capture these aspects. A mechanical model of this system should (1) properly represent the relative location of the events on the non-planar, complex fault surfaces, (2) include a background driving stress to load the system, and (3) determine the instantaneous static stress fields associated with each event.

2-1. Stress in a 3D dislocation simulation

We have developed 3D elastic crack models based on elastic half-space dislocation solutions [*Okada*, 1992] to model complex geometry and incorporate the full static stress interactions of the 655 RES events and ~5000 background earthquakes in the 1984 – 2004 observation period. The precisely relocated catalog of *Thurber et al.* [2006] with relative location uncertainties of nearby events estimated at 10s of m is utilized. For each earthquake source, we discretize a circular rupture patch into many small rectangular elements and impose an elliptical slip distribution to ensure a uniform stress drop. The rupture area (A) of the circular slip patch is derived using Hanks-Bakun scaling $A = 10^{(Mw-3.98)}$ [*Hanks and Bakun*, 2008] and the mean slip (D) over the patch is $D = M_0/(\mu A)$ where μ is the shear modulus. As shown in Fig. 3, the induced shear stress due to slip on the circular rupture patch (blue circle) is resolved on

different receiver planes. Positive stress changes result from RES events being in lobes of increased shear stress extending from the rupture edge and alongside the rupture at some distance from its center. On the horizontal plane through the center of the crack (Fig. 3b), the lobe-pattern of resolved horizontal shear stresses on vertical planes parallel to the crack reveals large negative stress, that is stress drop, (~ -10 kPa) in four lobes extending approximately one rupture radius from the patch and positive stress up to 9 kPa in four intervening lobes with a decaying pattern with distance. The lobe pattern is also evident in the vertical section shown in Figure 3d and 3e. On the vertical surface containing the crack (Fig. 3c), the solution for stress drop along the crack is noisy because of the numerical discretization. Thus within a distance of 0.1 rupture radius from the crack we assume the stress drop is equal to the imposed stress drop on the crack.

In this study, resolved shear stress is calculated on all 655 RES receiver events due to all M>1 source events at relocated 3D positions in the *Thurber et al.* [2006] catalog (4499 events). All source events are assumed to be strike-slip ruptures parallel to the average trend of the San Andreas fault (same strike and vertical dip), and horizontal shear stresses at receiver locations are resolved on vertical surfaces parallel to the fault and horizontal slip vector. The shear stress resolved on RES is shown in Fig. 4, where the separation distance between source (4110 background events) and receiver (655 RES events) is divided by source radius as "normalized distance". At first glimpse, both positive and negative stress reveals similar pattern of stress decaying with distance. As expected, the highest negative stress values occur within one rupture dimension (normalized distance <1). Within 5 rupture lengths (Fig.4b and 4d), 66.4 % of the values show positive stress change. Within one source dimension, however, there exists a dominance of negative stress changes (5045 events in total). For the short-DT events (< 5 days) that represent possible triggering, 94.3% have positive stress with maximum value of 6579 kPa at normalized distance = 0.4.

When the 3D stress results are compared with the 1D computation assuming $\Delta\sigma = 1/6\ \pi\ \mathrm{Mo}/r^3$ [*Aki and Richards*, 1980] (1D A&R stress), the largest difference occurs within one rupture dimension where large negative stress changes near 2000 kPa are computed in the 3D crack model, but very large stresses (> 10000 kPa) are obtained from the 1D computation (Fig. 5d). For normalized distance >1 the 1D A&R vs. 3D stresses generally follow 1:1 relationship (Fig. 5c). In addition, for the majority of positive stresses computed that are characterized by nor. distance >1 (only 49 events in nor. distance <1 in Fig. 5b), we found a bounding curve indicating 1:10 relationship between 1D A&R and 3D stress values (Fig. 5a). We suspect that the similar stress values for 1D A&R and 3D computation occur if events are close to the in-plane assumption (approximately parallel and aligned). In the 1D A&R stress computation in *Chen et al.* [2013] that neglects 3D geometry, the stresses are largely overestimated with opposite sign within one rupture dimension, while just outside one rupture dimension, the stresses are largely underestimated. Therefore, the very close-by events (nor. distance <1) are treated separately from the nor. distance > 1 case in the following analysis.

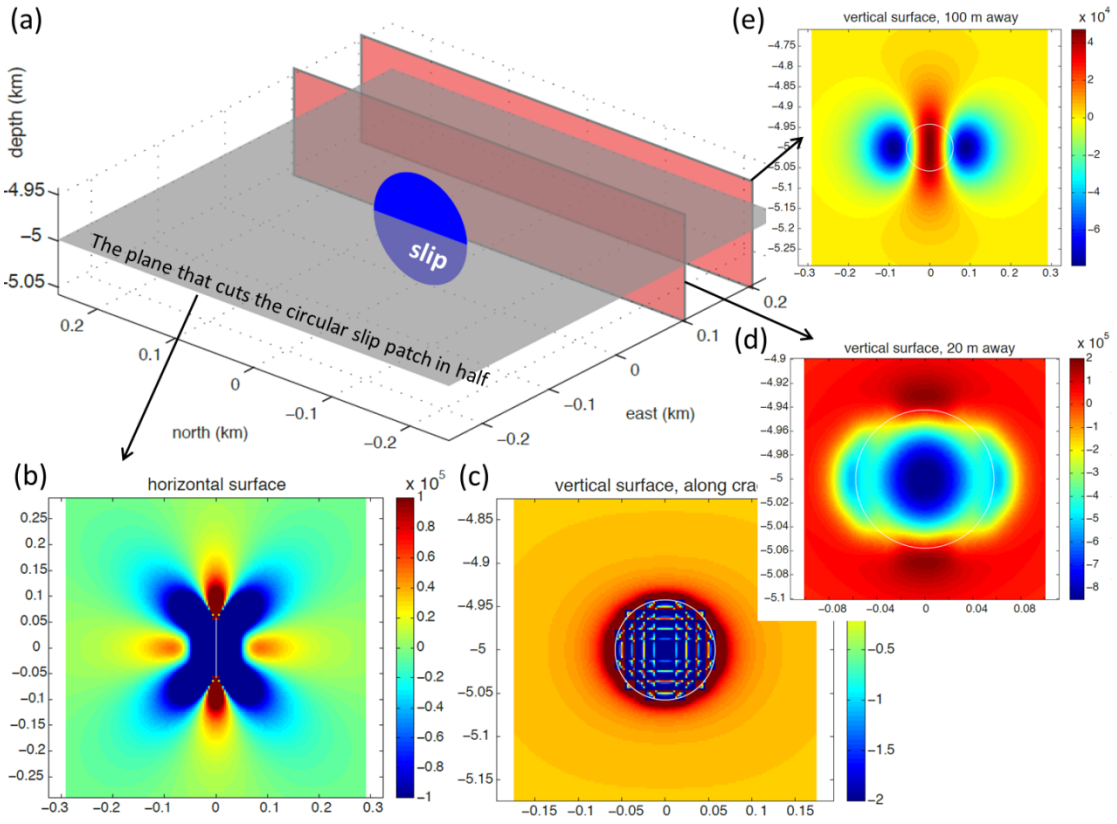

Figure 3. (a) Relative location of circular slip patch (blue circle) and resolved horizontal shear stress on vertical surfaces parallel to the crack. The horizontal plane (grey area) cuts the circular slip patch in half (b), while the vertical planes are parallel to the crack and shifted from the crack by 0 (c), 10 m (d), and 200 m (e). Stresses are in Pa and distances are all in km.

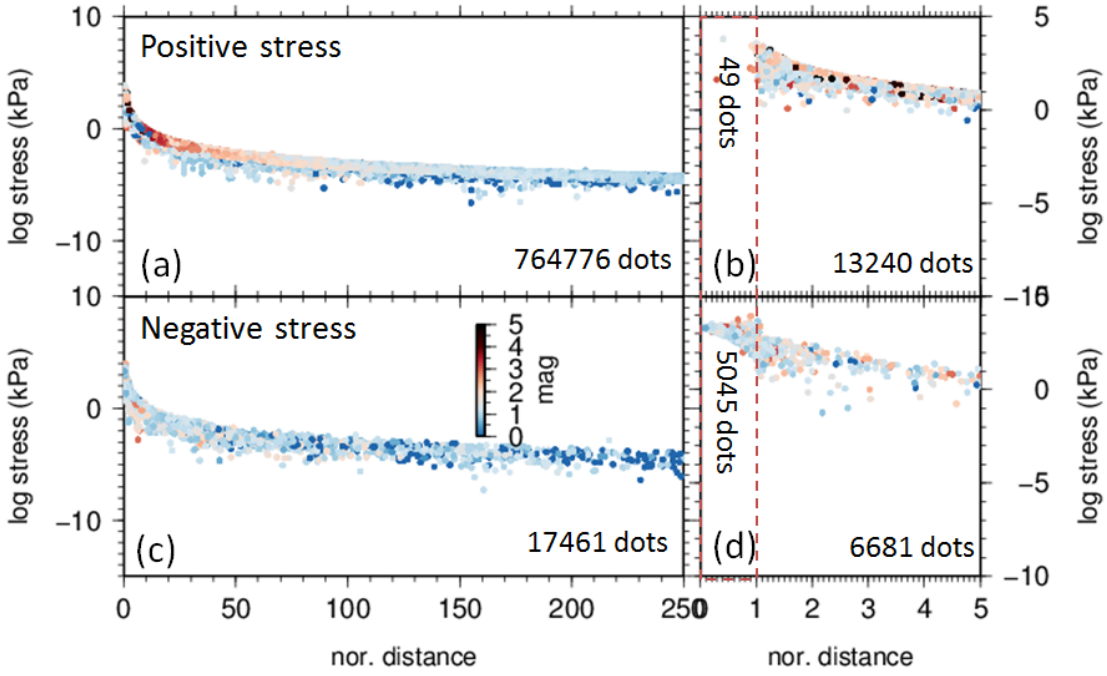

Figure 4. Positive (a-b) and negative (c-d) stress as a function of distance from the source, color-coded by magnitude of the source events. Red dashed line denotes the source-to-receiver distance equal to one rupture dimension.

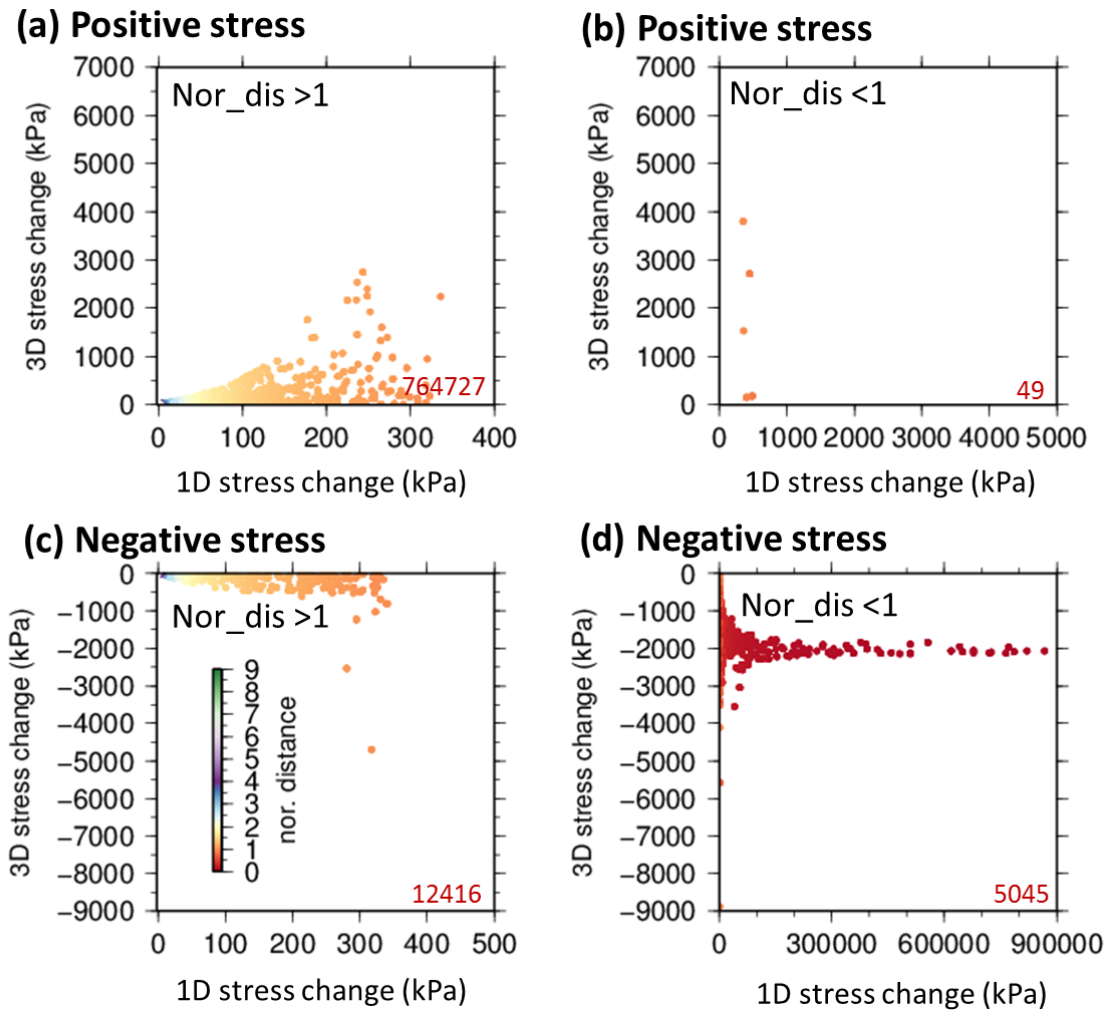

Figure 5. Stress computed using 3D dislocation (3D stress change) vs. stress using $\Delta\sigma=1/6\ \pi\ Mo/r^3$ [*Aki and Richards*, 1980] (1D A&R stress change) for (a-b) Positive stress and (c-d) Negative stress, color coded by normalized distance.

2-3. Velocity-strengthening afterslip contribution

In order to model the system of interacting earthquakes and surrounding aseismic creep, we also conduct a boundary element model of slip governed by rate-state friction. Following *Johnson et al.* [2013], we implement hierarchical matrix methods to efficiently compute the evolution of slip on the fault with a dense discretization. The models assume an isotropic, homogeneous and elastic half-space in which fault elements are discretized with rectangular patches. Non-steady creep on velocity-strengthening patches and episodic earthquake rupture on velocity-weakening patches is modeled assuming quasi-static deformation (no dynamic stresses). Earthquakes are modeled as uniform stress drop events on circular patches. The coseismic stress change on the fault is computed, and following *Mavrommatis et al.* [2014], we efficiently compute the evolution of aseismic slip (afterslip) on surrounding velocity strengthening regions assuming afterslip evolution is stationary in space and proportional to

fully relaxed afterslip. The time-dependence of afterslip is modeled using a simple analytical solution for a spring-slider model with velocity-strengthening friction. The time evolution of afterslip (δt) can be described by the equation below:

$$\delta t=\delta(t)\delta\infty=1+\sigma(a-b)k\delta\infty\ln\exp kV\infty t\sigma a-b-1+\exp-\delta\infty k\sigma a-b-V\infty t\delta\infty,$$

where $V\infty$ is interseismic loading rate, k is spring stiffness, σ is normal stress, a and b are the rate-dependent and state-dependent friction parameters. When time goes infinite the slip reaches the max. slip, which is presented by $\delta\infty$. The slip ($\delta\infty$) depends on the earthquake magnitude and is equal to the fully relaxed slip distribution. $\delta(t)$ depends on $\sigma(a-b)$, as illustrated by Fig. 6. The stress accumulation on the asperities is simply proportional to the normalized slip, as shown in the figure. Below we use $\sigma(a-b)$=0.1 as example.

In order to project seismicity into a fault plane, all Mw>1 events within one km of the SAF are collapsed onto the model fault plane and the stress changes on all 655 repeating events due to 3000 sources (out of ~4499 total M>1 sources) are computed. Each of the 3000 sources and all of the RES events are modeled with circular "asperities" on the fault that only slip instantaneously during earthquakes, while outside the asperities creeping is taking place on velocity strengthening regions. Circle radius is defined as above for the 3D crack solution (i.e., derived from Hanks-Bakun scaling A = $10^{(Mw-3.98)}$). The stress change due to on-fault sources (within 1 km from the fault plane) is computed including an instantaneous stress change plus contributions from afterslip (hereafter referred as 2D *co+af*). To understand the relationship between coseismic and afterslip induced stresses, we plot the ratio of total stress / coseismic stress in Fig. 7. We found that the afterslip stress is generally very small when coseismic stress is greater than 1 kPa, as denoted by quite small ratio in Fig. 7a. Very small coseismic events can have several times bigger afterslip stress, however, afterslip stress is reduced when coseismic stress grows (Fig. 7b). When afterslip stress > 1 kPa, however, the ratio grows significantly (Fig. 7c), indicating the afterslip stress is much bigger than coseismic stress in this category. This is also shown in Fig. 7d where events with very small coseismic stress can have several-times bigger afterslip-induced stress change; in contrast, the negative coseismic stress (generally produced when the receiver is located within one rupture dimension of the source) corresponds to smaller afterslip stress. Therefore we conclude that a small separation distance between the source and receiver leads to dominant coseismic stress, with relatively modest afterslip stress. The controlling factor of afterslip-induced stress will be discussed later in session 4.

When the 2D in-plane *co+af* stress results are compared with the prior computation using $\Delta\sigma=1/6\ \pi\ Mo/r^3$ [*Aki and Richards*, 1980] (1D A&R stress), we found that negative stress changes resolved within one rupture dimension (nor. distance <1) are mainly in a range of -1000 to -2000 kPa in 2D *co+af* model, corresponding to extremely large stress values in 2D computation (peak at 400

kPa) (Fig. 8d), while for nor. distance >1 the 1D A&R vs. 2D *co+af* stresses generally follow 1:10 relationship (Fig. 8c). With the majority of positive stresses computed being characterized by nor. distance >1 (only 852 events in nor. distance <1 in Fig. 8b), we also found a bounding curve indicating 1:15 relationship between 1D A&R and 2D *co-af* stress values (Fig. 8a). We found that in the 1D A&R stress computation in *Chen et al.* [2013] without considering afterslip process, the stresses are largely overestimated with opposite sign within one rupture dimension, while outside one rupture dimension, the stresses are largely underestimated for both negative and positive stresses. As a result, 18% of the very close-by events (nor. distance <1) are underestimated in 1D A&R stress (Fig. 8b) and 82% are in the stress shadow (Fig. 8d). For events outside one rupture dimension, the stresses are largely underestimated. The role of stress shadow computed in the in-plane 2D solution will be computed and compared with 3D dislocation in the following analysis. Note that afterslip itself produces only positive stress. When the source is located in an immediate neighborhood, the afterslip stress is confined within 300 kPa (Fig. 9b), whereas outside one rupture dimension we expect much bigger stress compared with 1D A&R method (Fig. 9a).

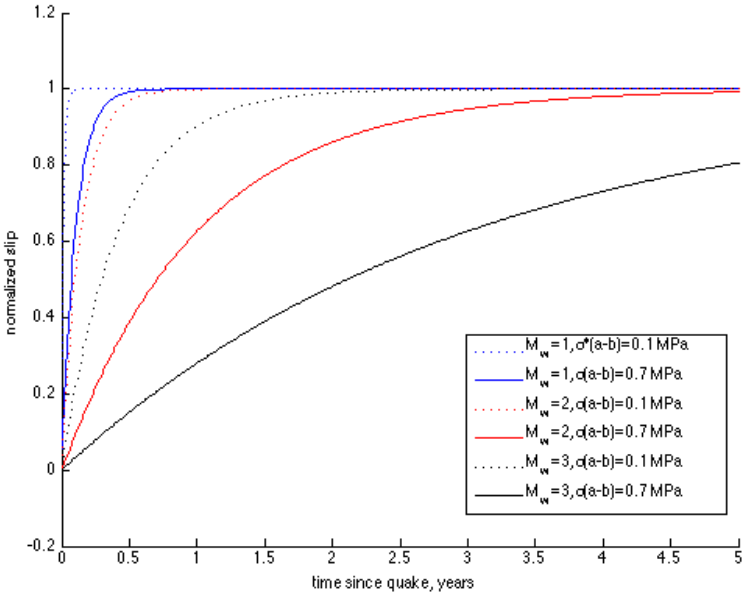

Figure 6. Afterslip evolution with time computed for a spring-slider model for different friction parameters.

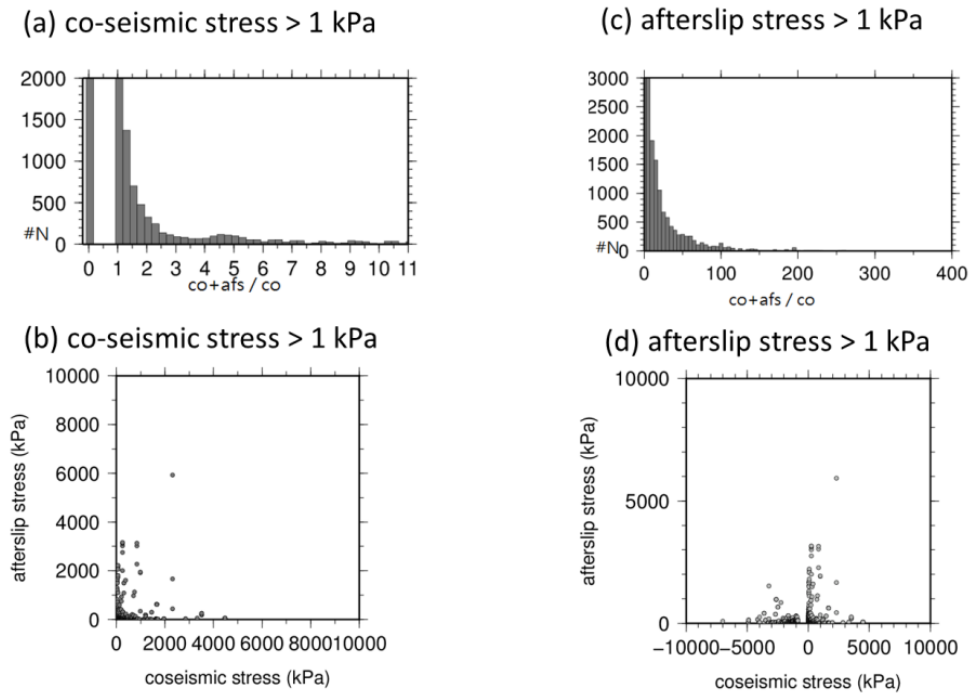

Figure 7. (a-b) Histogram of total stress(*co+af*)/coseismic stress and plot of total stress vs. coseismic stress for coseismic stress greater than 1 kPa. Note that zero stress is given if the time of the source (background events) is after the time of the receiver (RES events). (c-d) Histogram of total stress /coseismic stress and afterslip stress vs. coseismic stress plot for afterslip stress greater than 1 kPa.

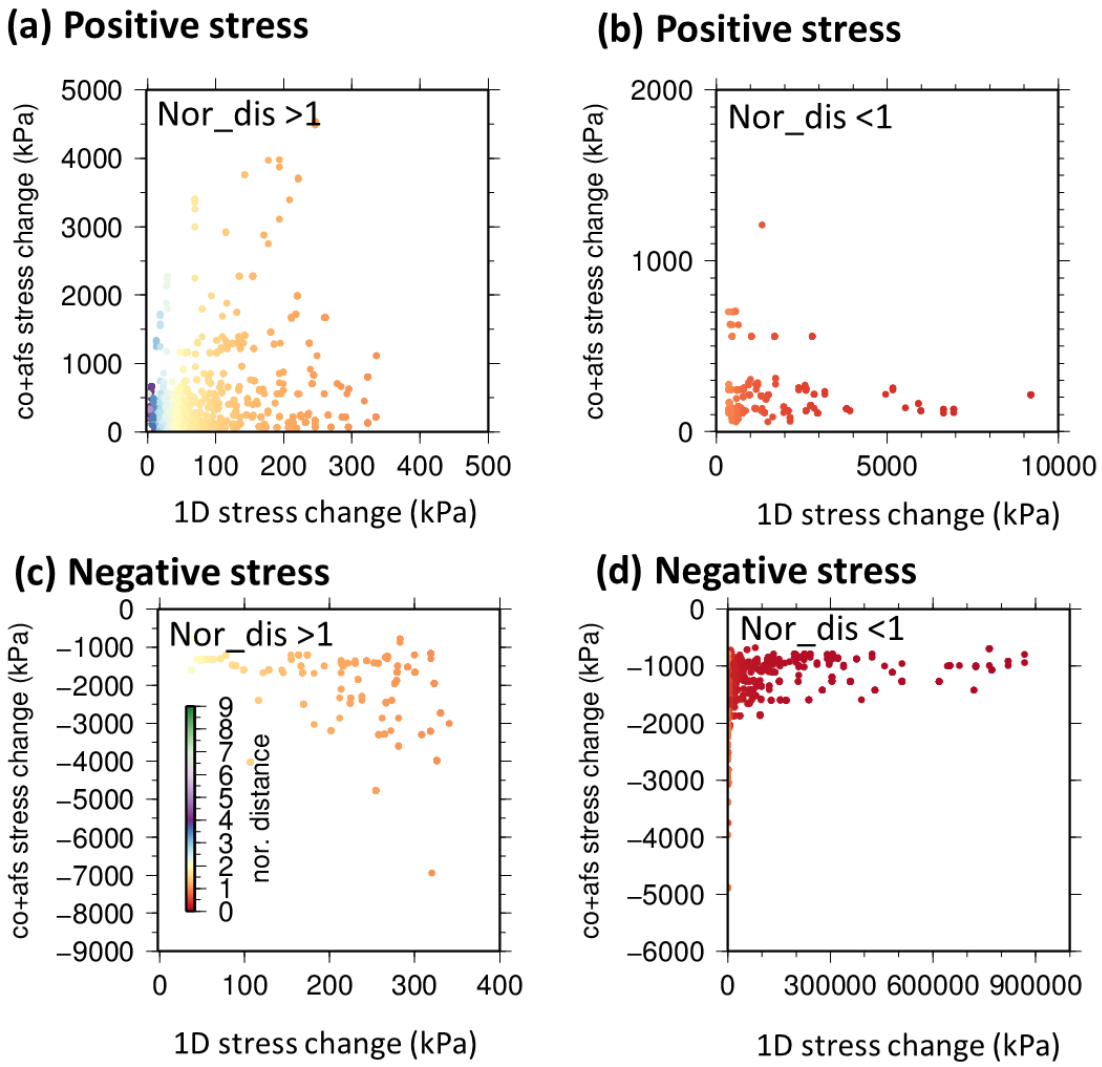

Figure 8. Stress computed using 2D *co+af* model vs. stress using $\Delta\sigma=1/6\ \pi\ \mathrm{Mo}/r^3$ [*Aki and Richards*, 1980] (1D A&R stress change) for (a-b) Positive stress and (c-d) Negative stress, color coded by normalized distance.

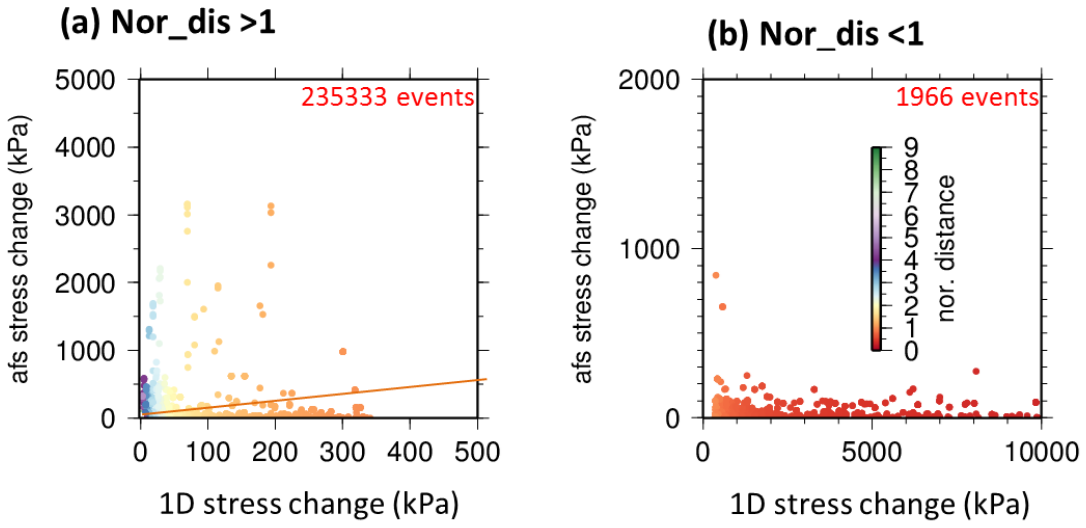

Figure 9. Stress computed using 2D *afterslip* model vs. stress using $\Delta\sigma=1/6\ \pi\ Mo/r^3$ [*Aki and Richards*, 1980] (1D A&R stress change) for normalized distance greater than 1 (a) and shorter than 1 (b). Orange lines indicate 1:1 relation.

3. Role of stress shadow in earthquake interaction?

3.1 3D crack model

(1) Normalized distance less than 1

As addressed in section 2, we have discovered that within one rupture dimension, the stresses treated as extremely large positive stress using a simplified $\Delta\sigma=1/6\ \pi\ Mo/r^3$ in the prior study [*Chen et al.*, 2013] should be in a stress shadow instead. Among 5094 stress calculations measured for nor. distance < 1, 99% of them reveal negative stress. To understand how the negative stress affects the variability of recurrence interval, we first explore whether the static stress change experienced by RES during a given recurrence interval correlates with the length of that interval. Here the time spanned by a recurrence interval is normalized by the average recurrence interval (Tr) for the respective sequence and plotted against the external stress change taking place during that period. As shown in Fig. 10a, the population of RES that experienced stress change greater than 100 kPa have a mean normalized Tr of 0.99 (median value 0.93), this value remains near 1 under $>10^4$ kPa. However, if the stress changes are divided by the recurrence interval as "stressing rate", there appears a linear trend of normalized Tr decreases with increasing stressing rate. Under $>10^4$ kPa/yr, the mean and median normalized Tr becomes 0.63 and 0.59, respectively, suggesting a significant reduction of Tr by high stressing rate instead of stress change. The notable reductions in Tr produced by the largest negative stressing rate may indicate (1) the very high and negative stress-change values are in fact events where we incorrectly model the RES as falling in stress-drop regions and/or (2) triggering by nearby events is actually dynamic, in which case we would expect short *DT* for very close, very-high absolute stress

(positive or negative). However, we do not find evidence that indicates shorter *DT*, higher stress from preshocks statistics.

(2) Normalized distance greater than 1

Outside one rupture dimension, negative stresses are also sometimes measured, which reveal similar values with the ones by the simplified $\Delta\sigma=1/6\ \pi\ \mathrm{Mo}/r^3$ in the prior study [*Chen et al.*, 2013]. Among 777143 stress calculations measured for nor. distance > 1, only 1.6% reveal negative stress, while the 99.4% show positive stress that is about 10 times bigger than 1D A&R stress model in *Chen et al.* [2013]. As shown in Fig. 11, the population of RES that experienced positive and negative stress change greater than $>10^3$ kPa and $>10^3$ kPa/yr have a shorter normalized Tr compared with the events that experienced smaller stress. Note that in the middle panels of Fig. 11, the negative stresses reveal somewhat more significant reduction in Tr under greater stress loading ($>10^3$ kPa and $>10^3$ kPa/yr), which may not be statistically meaningful due to the relatively small number of events (<10). When the normalized Tr is plotted as a function of the RES's COV (coefficient of variation in recurrence interval) (Fig. 12), we find that the majority of events that experienced $>10^4$ kPa/yr have relatively lower normalized Tr (<1), suggesting a modest shortening of a recurrence interval by extreme stress perturbations. This stress increment is consistent with the value inferred in *Chen et al.* [2013], indicating the required stress change for significant shortening in RES's recurrence interval remains the same with or without considering the effects of 3D geometry. Also note that the increasing COV reflects the spread of Tr for a given sequence (vertical alignment indicates the same sequence).

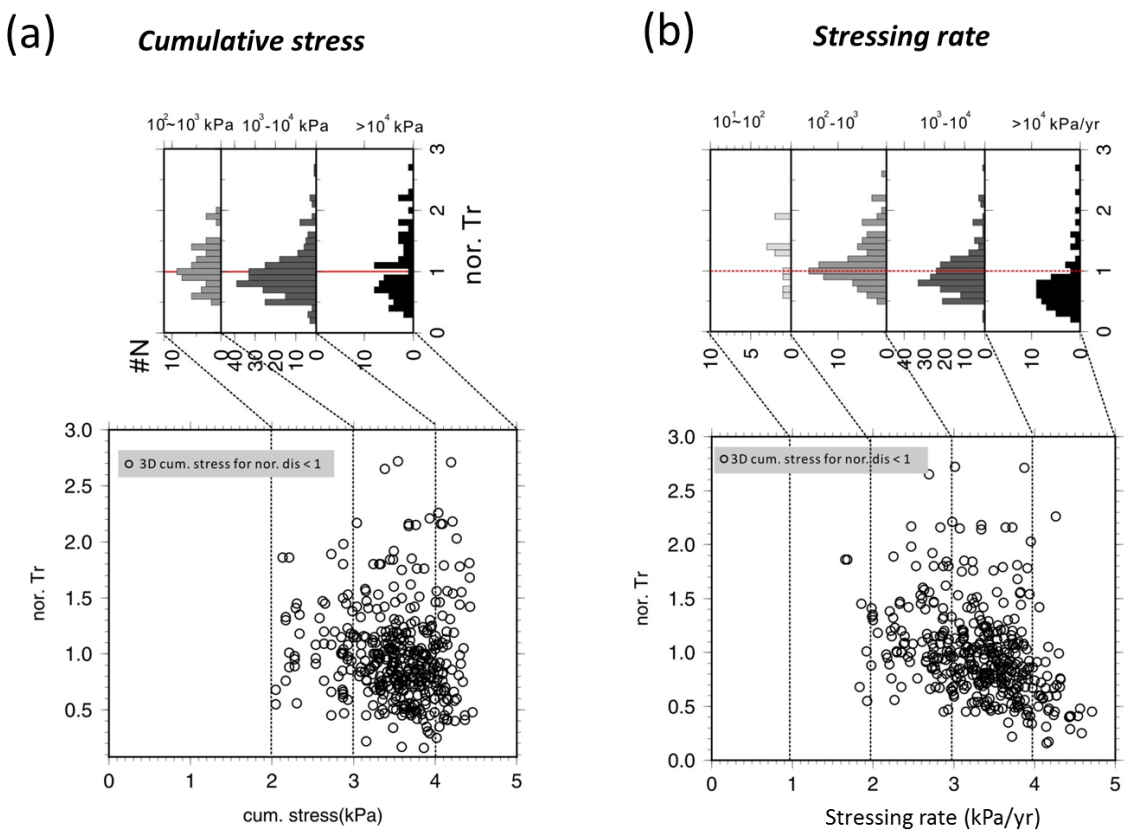

Figure 10. Results for 3D crack model. Normalized recurrence interval (Tr) of RES events as a function of (a) stress change and (b) stressing rate during the preceding recurrence interval for events within normalized distance < 1 of the source event. Upper panels show histograms of normalized Tr for different ?negative? stress change / stressing rate ranges.

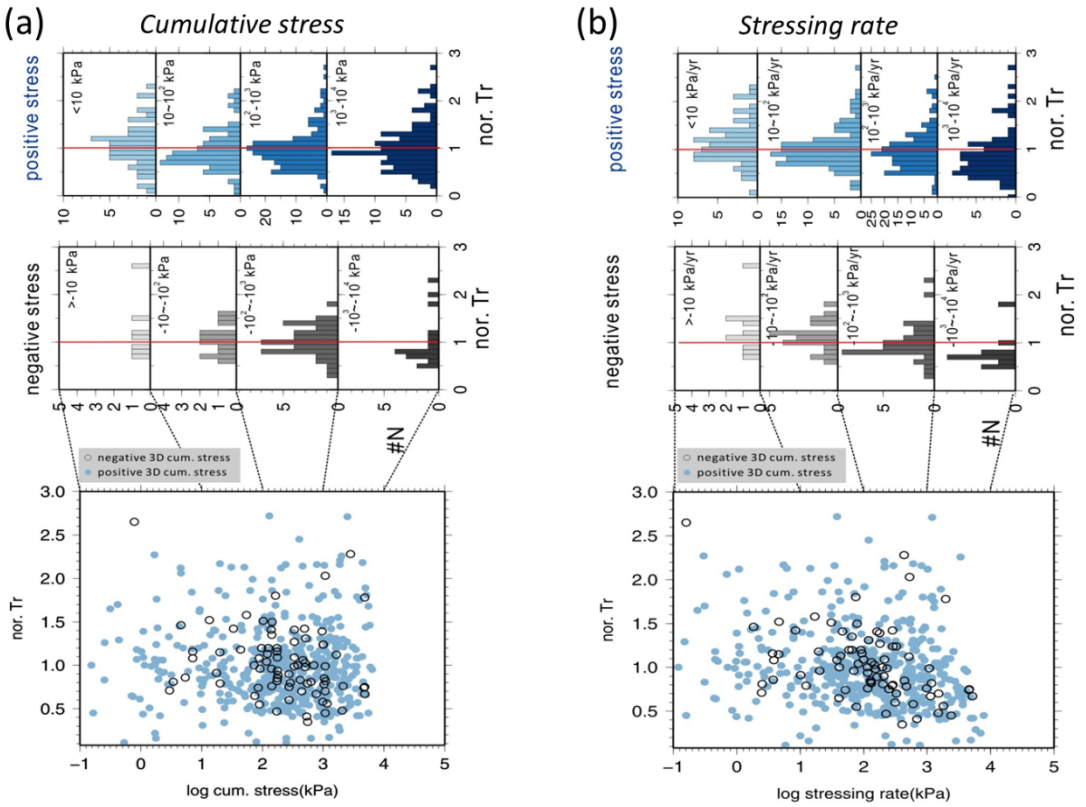

Figure 11. Results for 3D crack model. Normalized recurrence interval (Tr) of RES events as a function of (a) stress change and (b) stressing rate during the preceding recurrence interval for normalized distance >1. Upper and middle panels show histograms of normalized Tr for positive and negative stresses, respectively. The lower panels show normalized Tr vs. stress and stressing rate, with open symbols being events for which computed stress-change values were negative.

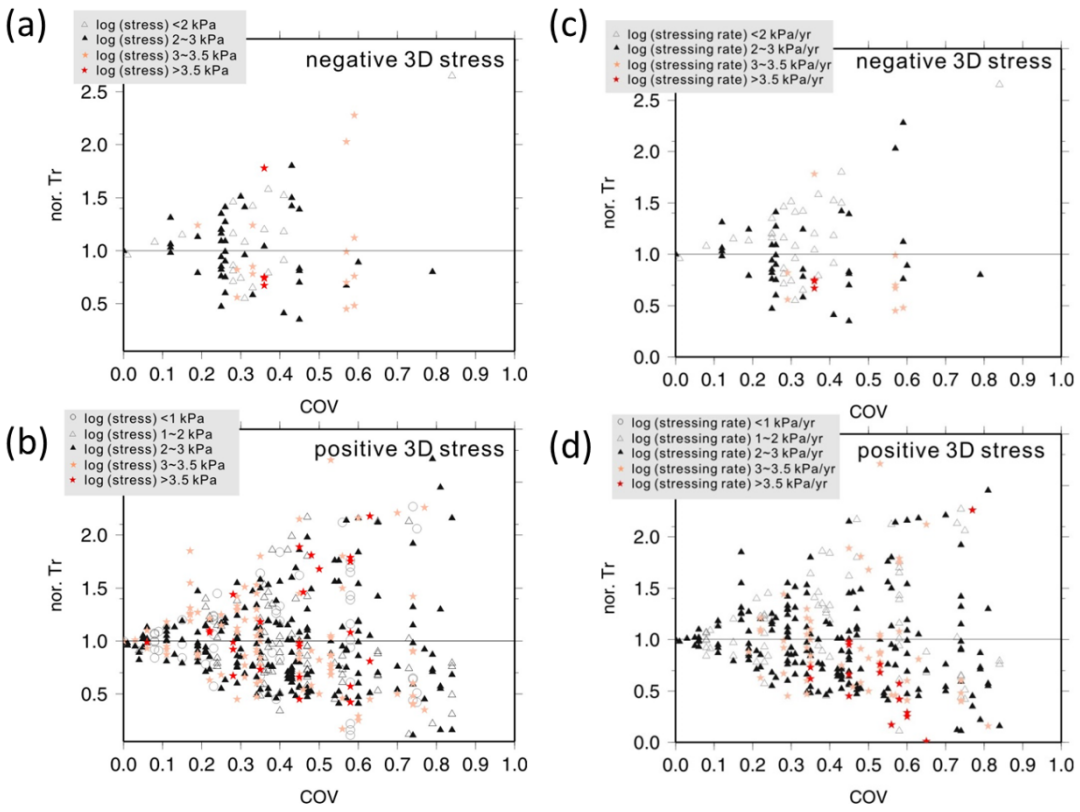

Figure 12. Normalized Tr values versus COV of each RES. Here only normalized distance > 1 events are computed. The RES events exposed to different ranges of stress change and stressing rate are shown by different symbols.

3.2 2D dislocation model

(1) Normalized distance less than 1

When the 2D in-plane model with afterslip is applied, there exists majority of negative stress within one rupture dimension. To understand the role of these negative stresses on RES's recurrence interval, we plot the normalized Tr as a function of computed stresses in Fig. 13. We found that the population of RES that experienced $>10^4$ kPa/yr stressing rate have a shorter normalized Tr compared with the events experienced smaller stressing rate, consistent with the pattern computed using 3D dislocation model. The cumulative stress however, does not reveal such trend.

(2) Normalized distance greater than 1

Outside one rupture dimension, the negative stresses are also measured. The negative stresses are about 10 times greater than the ones determined by the simplified $\Delta\sigma=1/6\ \pi\ Mo/r^3$ in the prior study [*Chen et al.*, 2013], which is about 10 times bigger than the 3D stress model in Fig. 5c, indicating the in-plane assumption may overestimate the stress change. Among 588794 stress calculations measured for nor. distance > 1, only 0.1 % of them reveal negative stress. The negative stress however, does not reveal significant reduction in Tr as shown in the middle panels of Fig. 14. Also shown in Fig. 13, the population of RES that experienced positive and negative stress change greater than $>10^1$ kPa

and >10^1 kPa/yr have a shorter normalized Tr compared with the events experienced smaller stress. Though the degree of the Tr-shortening in is not as significant as the one reveal in 3D stress computation.

Consequently, the negative stresses not considered in Chen et al. [2013] are found to be dominant in one rupture dimension (normalized distance < 1) for both 3D and 2D dislocation stress models. 99% and 82% repeaters are loaded by negative stress from their neighbors for 3D and 2D cases, respectively. Given these negative stresses play only a small portion in all stress population (smaller than 0.1%), they do not "lengthen" with high stress as expected for stress shadow hypothesis. Instead, there exists shortened interval for high stressing rate. This suggest (1) the very high and negative stress-change values are in fact events where we incorrectly model the RES as falling in stress-drop regions and/or (2) triggering by nearby events is actually dynamic, in which case we would expect short *DT* for very close, very-high absolute stress (positive or negative).

The majority of the stress calculations are for events at normalized distances greater than 1, which are also analyzed for their Tr-shortening behavior vs. stress change. We find that the stresses are largely underestimated using the A&R relation in Chen et al. [2013], both 3D and 2D dislocation models support that the real stress should be about 10 times bigger. The positive stress events are shortened by high stressing rate with the threshold at $10^{3.5}$ kPa in 3D dislocation model , which is three times higher than that determined using A&R relation. Consequently, the required stress changes for significant shortening in RES's recurrence interval should be higher when the 3D geometry is considered.

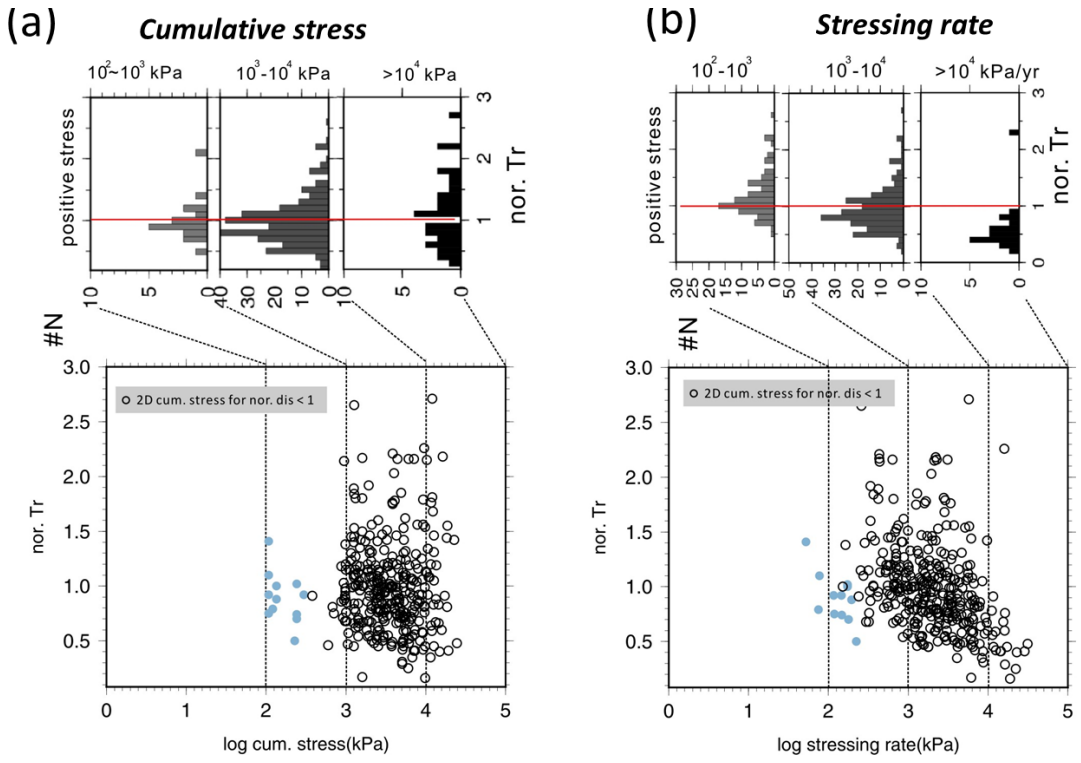

Figure 13. Results for 2D model. Normalized recurrence interval (Tr) of RES events as a function of (a) stress change and (b) stressing rate during the preceding recurrence interval for normalized distance <1. Upper and middle panels show histograms of normalized Tr for positive and negative stresses, respectively.

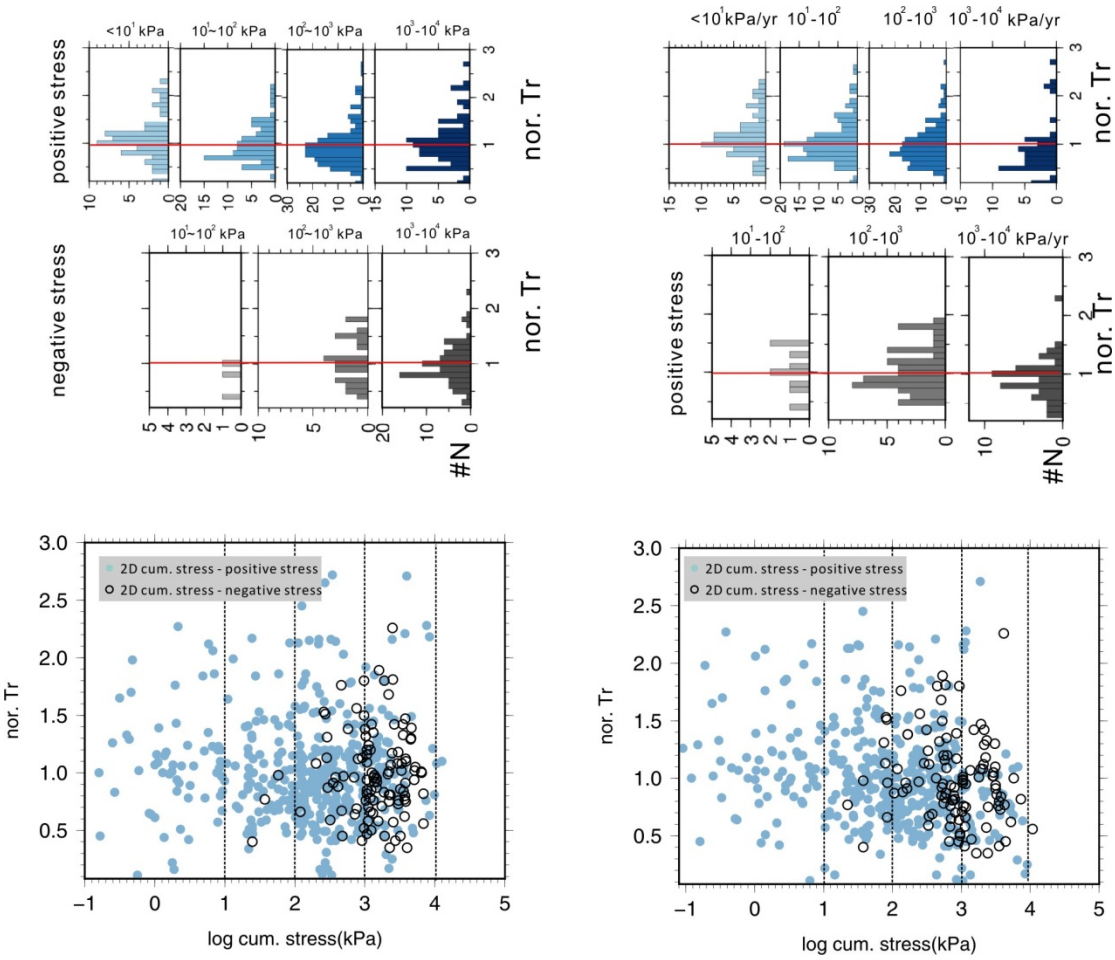

Figure 14. Results for 2D model. Normalized recurrence interval (Tr) of RES events as a function of (a) stress change and (b) stressing rate during the preceding recurrence interval for normalized distance >1. Upper and middle panels show histograms of normalized Tr for positive and negative stresses, respectively.

4. Role of afterslip in earthquake interaction

In our velocity-strengthening afterslip calculations, afterslip outside of the asperities produces up to 30 times larger stresses compared with that determined from A&R relation (Fig.9a). The afterslip stress is therefore regarded as an important contributor to our stress computations that has been neglected both in former A&R calculation and 3D dislocation model. To understand the role of afterslip stress in earthquake interaction, we next discuss under which condition the afterslip induced stresses are significant.

In Fig. 15, we calculate the number of neighboring earthquakes from each repeating sequence (in a distance of 5km) and the cumulative afterslip induced stresses. Within one rupture dimension, the afterslip stresses are smaller (confined within 1200 kPa) (Fig. 15a). When the sources are located outside the rupture dimension of receiver (RES), however, the afterslip stress appears to be bigger when there are less nearby events (Fig.15b). This suggests that the crowdedness of nearby seismicity may influence the afterslip stress. When the freely sliding area is relatively bigger (less crowded), the afterslip induced stress tend to be bigger. These afterslip induced stresses tend to occur outside one rupture dimension of the source and is found to be much bigger than previously determined in A&R relation (Fig. 9a) and 2D coseismic stress (Fig. 7c). This should be carefully considered in the future stress computation and the understanding of earthquakes interaction.

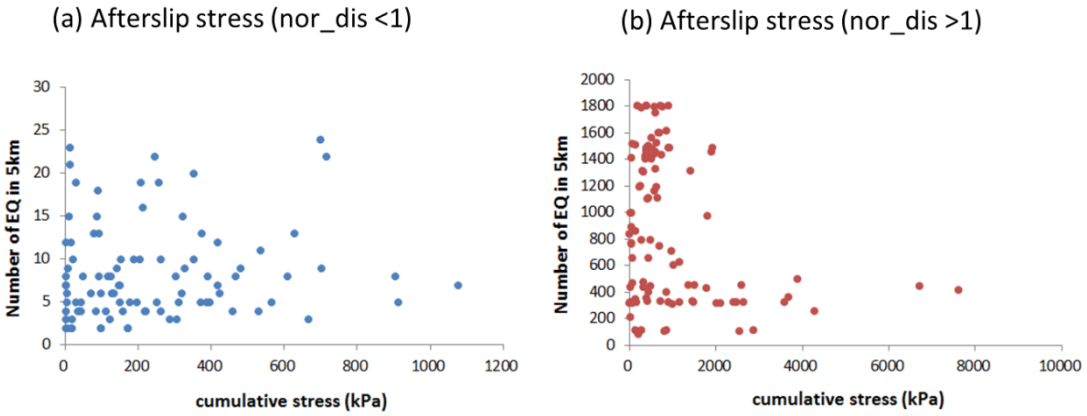

Figure 15. The number of earthquakes in 5 km each RES as a function of cumulative afterslip stresses for (a) normalized distance < 1 (b) normalized distance < 1.

B. Update of SAFOD Zone Repeating Earthquakes

Based on more than a decade of work that established a detailed record of micro-earthquakes with data from the borehole HRSN network and surface NCSN network sites at Parkfield, we have improved the observational constraints of the background and RES event data within a cubic 1.5 km volume containing the SAFOD target region by (1) increasing catalog completeness using template cross-correlation scanning techniques, (2) improving consistency and precision of the relative spatial distribution of the background and repeating earthquakes by incorporating cross-correlation alignments in a single double-difference joint relocation inversion, and (3) by taking advantage of waveform similarity and the close proximity of the clustered events to constrain their relative sizes using low frequency spectral ratios (proportional to the relative seismic moments of the events).

Within the 1.5 km volume, waveforms for one event from each of the 17 repeating sequences, initially identified in the SAFOD volume, were used as

templates for detection of additional events and phase-alignments (colored symbols in Fig. 16). As of Dec 31, 2015, 2586 events were detected within this volume. However, many of these events were detected by one or more of the templates. A procedure for removing the duplicate events was developed that retained events with the best template cross-correlation match, reducing the number of uniquely identified events to 1220 events within the 1.5 km dimension volume. High-precision double-difference relocations of the 1220 events was carried out in a joint inversion using 5,388,326 catalog and cross-correlation phase-alignment pairs. Of the 1220 events, 316 were found to be characteristic repeats of one of the original 17 repeating sequences. Many of the remaining 900+ events also appear to be characteristic repeats of other small magnitude sequences, and their formal identification and organization into repeating sequences is planned.

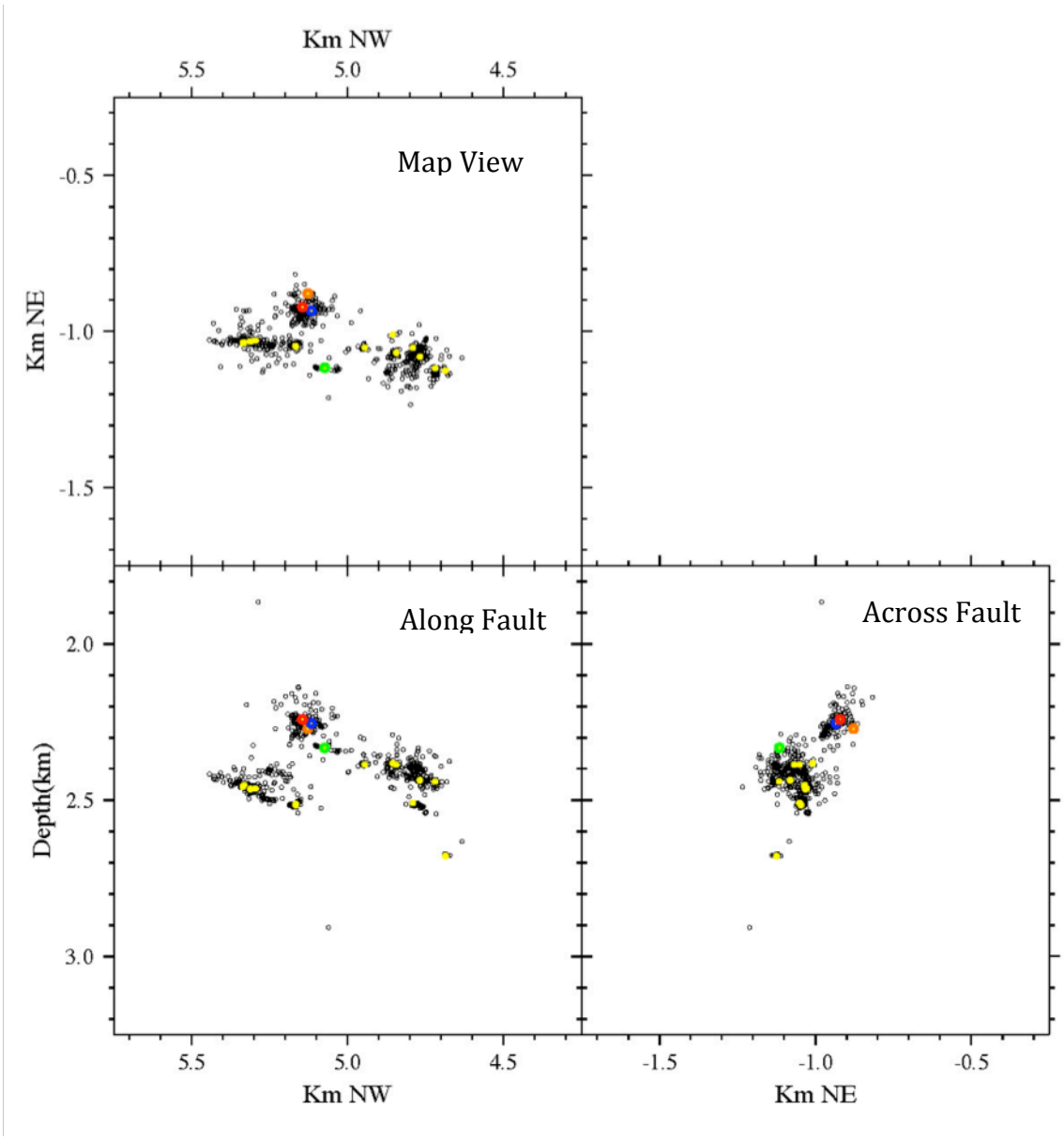

Figure. 16. Cubic volume (1.5 km dimension) containing the 1220 repeating and background events in the SAFOD target region catalog. Locations are from joint double-difference relocations. Colored symbols are sites of the 17 characteristically repeating sequence in the volume. SF, M1, LA, and HI sequences are colored red, orange, blue and green, respectively. The remaining sequences are colored yellow and background events are open gray circles. Seismicity in the volume is strongly clustered and reveals substructures that are primarily distributed along strike, but are also distributed laterally to some degree.

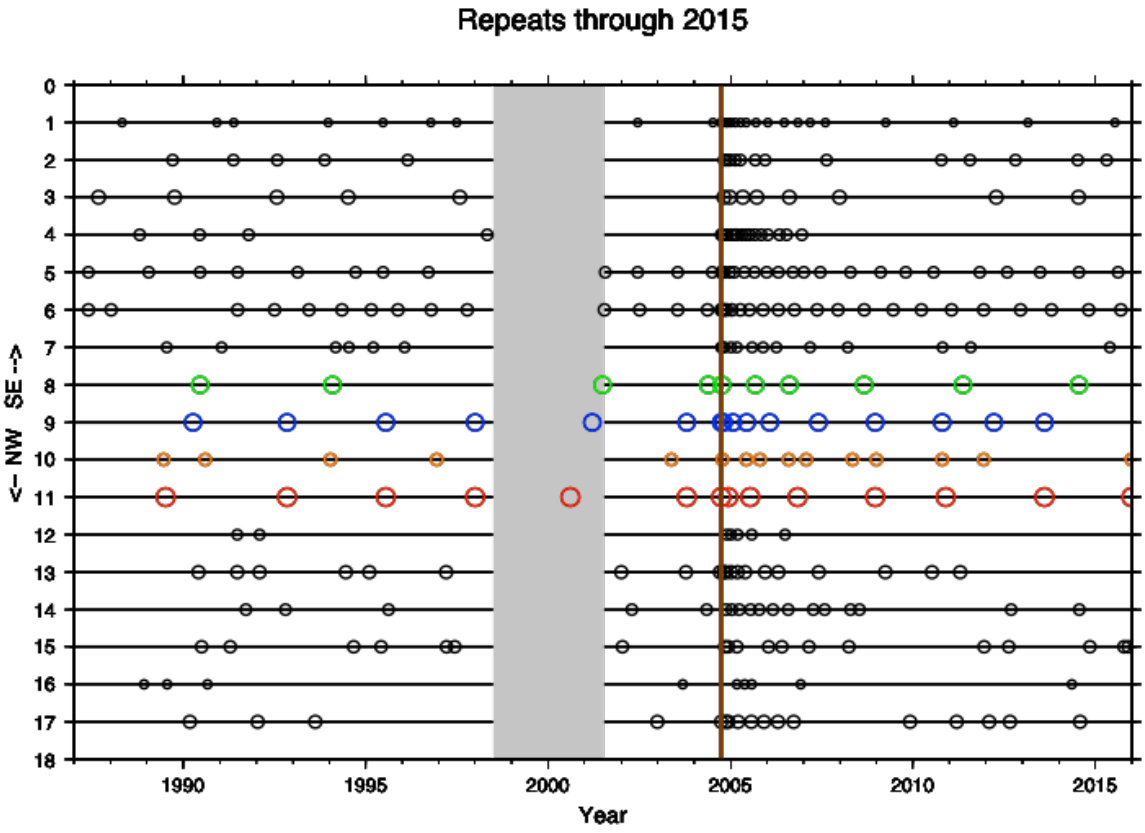

Figure 17. Recurrence histories of the 17 characteristic sequences initially identified in the SAFOD target volume, ordered from SE to NW along SAF strike. Green, blue, orange and red colors are as in **Fig. 16**. Gray band is period when HRSN data was not available. Repeats of the SF, LA and HI sequences during that period were determined using the USGS's surface NCSN network. Brown vertical line is time of the 2004 Parkfield M6, mainshock.

In Figure 17 the updated recurrence histories of the confirmed 17 target repeating sequences are shown. The updated scan-based cross-correlation method provides the most complete catalog of the times and magnitudes of the characteristically repeating sequences, because detections are based on scanning through continuous records and do not depend of preexisting detection catalogs. The identification of future repeats of these frequently recurring small magnitude sequences using the scanning methods we have developed also holds the potential for testing of interaction based time dependent earthquake forecast models by allowing forecasts of the next repeat to be made and comparisons of success rates when a repeat is realized.

Using the most updated repeating earthquake catalog, we have tracked the temporal variation of interaction between sequences that are very close in space. Fig. 18a shows the relative location of the SAFOD SF, LA, and HI sequences,

whereas Fig. 18b-c shows the event chronologies from these sequences. Average magnitudes for the SF, LA, and HI sequences are M2.1, M1.8, and M1.8 and their corresponding average recurrence intervals during the 1984-2014 time period are 2.0895, 1.6978, and 2.5071 yr. The SF and LA sequences are located within 50 m of each other and their time histories reveal high similarity, with small time separations ranging from 18.04 s to 0.75 yr, before the 2004 M6 Parkfield (Fig. 18b). During this pre-2004-mainshock period, the larger-magnitude SF sequence events always occurred shortly before the LA events, establishing a relatively consistent triggering pattern between the two sequences. Immediately after the Parkfield event, however, this relationship breaks down, with LA either occurring shortly before SF or without any apparent trigger relationship with SF (Fig. 18c). By ~ 9 years after the Parkfield mainshock, the original SF-leading LA trigger pattern appear to possibly be returning. What controls the interaction between SF, LA, and HI sequences? Can we find a causal relationship between the directionality of triggering between them, possibly related to the role of aseismic creep? And what are the roles of static stress, loading rate, aseismic slip, and frictional properties of the asperity on the interaction? These questions can be further evaluated by careful updated observations of the target events and nearby smaller earthquakes and stress modeling considering the complex multi-strand fault geometry and frictional fault slip.

At the first year of this project, however, we have not yet included time-dependent stress changes associated with aseismic afterslip following each event while employing a failure stress condition that determines when an asperity fails, in order to explain the time histories of SAFOD target sequences. Our next plan is to model the timing of RES events and the potential stress interactions with nearby events allowing earthquakes to rupture naturally on asperities. Since it would be difficult to model exact RES event histories with this approach, we will instead treat this type of modeling as more of a parametric study in which we generate repeating earthquake sequences and examine the extent to which the observables such as Tr, DT, and Mo, and model rate-state friction are influenced by the choice of rate-state friction parameters and the geometry (size, spacing) of RES events. We plan to conduct this type of simulation for comparison with observations of the SAFOD target sequences in the near future.

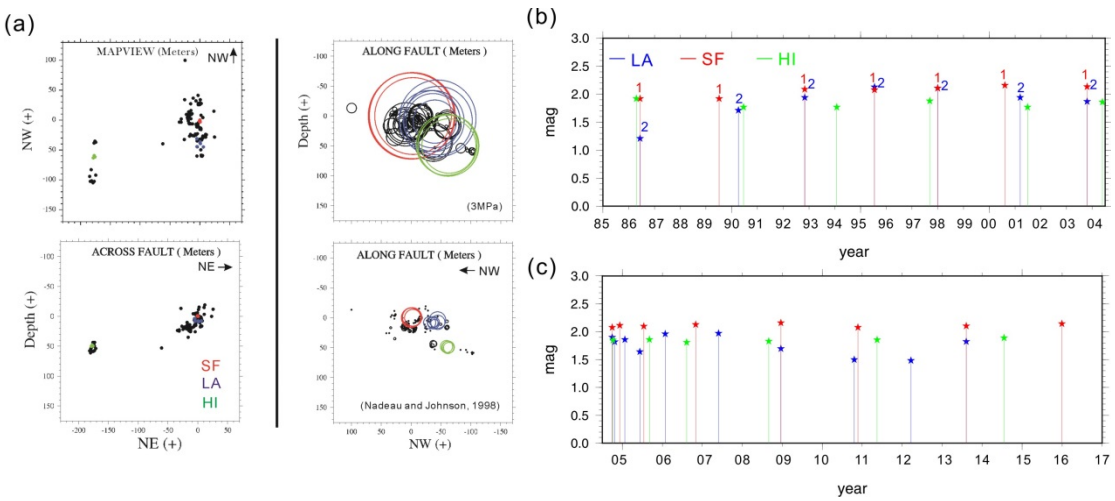

Figure 18. (a) (left) Map view of and across-fault double-difference relocations of the SAFOD target cluster: SF (red), LA (blue), and HI (green) ~M2 SAFOD target sequences. Black dots indicate the nearby repeating sequences (black). Relative relocations of the repeating events in the SAFOD target region occurring since August of 2001 are determined using hypoDD and sub-sample precision cross-correlation alignments. (Right) Along fault cross-section showing rupture dimension assuming a stress drop of 3 MPa (top) and the dimension suggested by *Nadeau and Johnson* [1998] (bottom). (b) Event chronologies for pre-PK repeating events in SF (red), LA (blue), and HI (green). Numbers indicate the order of SAFOD target sequences occurrence in one year. (c) Event chronologies for post-PK repeating events.

C. Finite-source Slip Inversions of the Repeating SAFOD M2 SF Sequence

In general and for the stress modeling used in this project, slip and associated stress over the entire rupture dimension is assumed to be uniform. Recent observational, and modeling studies suggest, however, that this may not be the case (*Johnson and Nadeau*, 2002 and 2005; *Dreger et al.*, 2007; *Chen and Lapusta*, 2009; *Johnson*, 2010). To aid in the interpretation of our mechanical modeling effort, we also participated in finite-source inversion efforts of the SF (San Francisco) M2 repeating earthquake sequence from the San Andreas Fault Observatory at Depth (SAFOD) experiment. This work was in collaboration with Ahyi Kim of Yokohama City University in Japan and Douglas Dreger and Taka'aki Taira of U.C. Berkeley (*Kim et al., 2016*).

Using the precise relocations, and seismic moments from our SAFOD target volume catalog of repeating and background events we identified suitable eGf events and the relative positions of the SF sequence to perform and verify full-waveform finite-source slip inversions for eight of the SF sequence events occurring before and after the 2004 Parkfield mainshock (Fig. 19 and Fig. 20). Results of the analysis showed that rather than being uniform, slip and stress-drop during the SF events was highly variable on their rupture patches, but that the pattern of variability was relatively consistent among the events. An unexpected additional result of the study was that the peak of slip/stress-drop of the inversions showed a modest, but significant reduction for

the SF events immediately following the Parkfield M6 and a subsequent recovery of peak values as time progressed following the M6 mainshock. These results have given us a clearer understanding of the role of heterogeneity in earthquake slip and stress and how such heterogeneity may affect our stress modeling results.

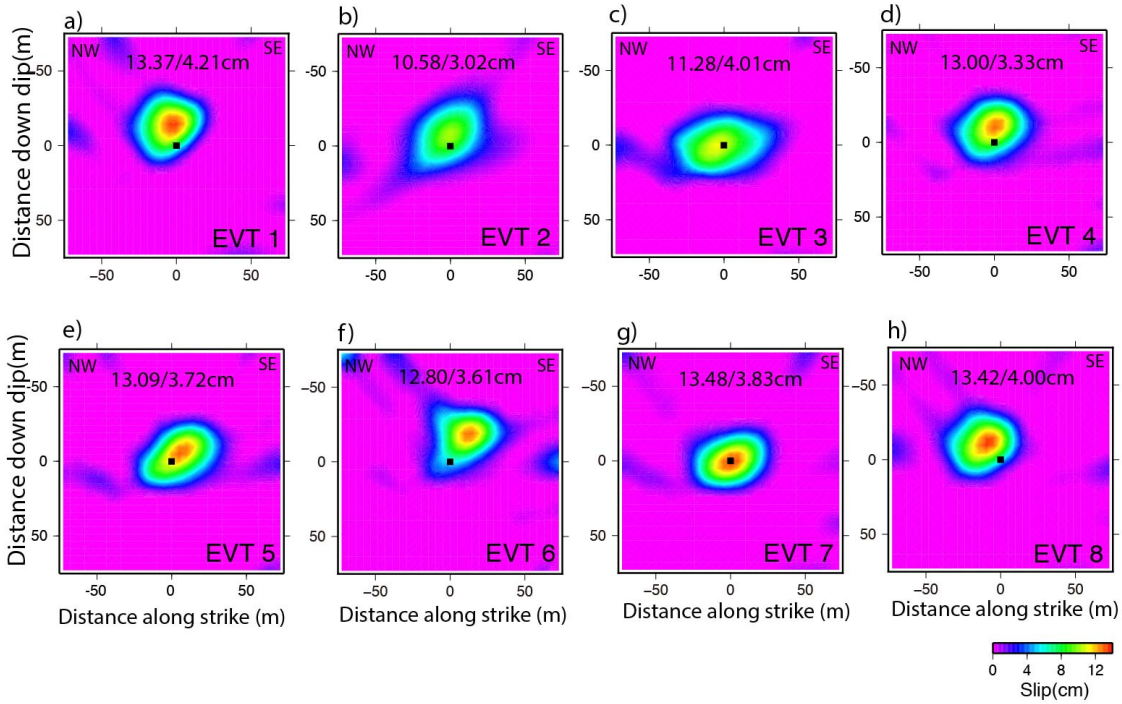

Fig. 19. Comparison of best-slip models obtained for the eight SAFOD repeating events using eGfA. The black square indicates the hypocenter. (a) EVT1. (b) EVT2. (c) EVT3. (d) EVT4. (e) EVT5. (f) EVT6. (g) EVT7. (h) EVT8. The two numbers in each panel indicate the peak and average slip of the main asperity for each event, respectively.

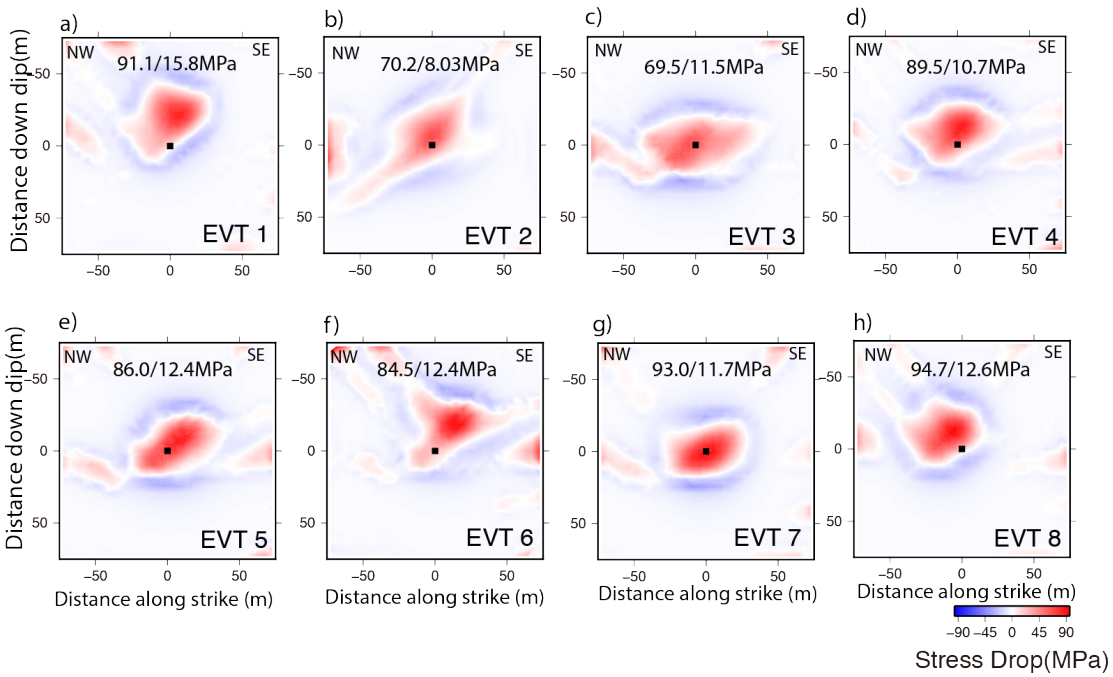

Figure 20. Comparison of stress drop distribution obtained for the eight SAFOD repeating events using eGf A. (a) EVT2. (b) EVT3. (c) EVT4. (d) EVT4. (e) EVT5. (f) EVT6. (g) EVT7. (h) EVT8. The two numbers in each panel indicate the peak and average stress drop for each event, respectively.

D. Relating Transient Seismicity to Episodes of Deep Creep at Parkfield CA

Ultimately, an understanding the interaction of stress-transfer and its evolution on a larger scale is critical to improving the implementation of fault interaction physics into the development of time dependent earthquake probability estimates. To this end, in collaboration with Charles Sammis and Rachel Lippoldt of USC and Stewart Smith (retired), we also participated a complementary study relating transient seismicity to episodes of deep creep from repeating earthquakes, non-volcanic tremor, coulomb stress transfer and the 2004 Parkfield M6 mainshock (*Sammis et al., 2016*).

In addition to our repeating earthquake data for the Parkfield region, this study collected and compiled data on seismicity, source mechanism, creep, low-frequency events (LFEs) from a variety of sources and generated a non-volcanic tremor catalog for the Parkfield area extending back to 1994. These data were then analyzed and used to develop a coulomb stress change model for comparison with the overall pattern of seismicity and change through time.

The study found that the 2004 M6 Parkfield CA earthquake was preceded by a four-year period of anomalously high seismicity adjacent to, but not on, the San Andreas Fault. The rate of small events (Mw<3) at distances between 1.5 and 20 km from the fault plane and at depths greater than 8 km increased from 6 events/yr prior to 2000 to 20 events/yr between 2000 and the 2004 earthquake. This increase in seismicity coincided with an increase in the rate of non-volcanic tremor, which, if

tremor is indicative of creep on the fault plane, suggests that creep may have driven the enhanced seismicity. Coulomb stress transfer calculations predict the observed spatial pattern of the seismicity, and thus support a causal relation between creep at the base of the fault zone and off-fault seismicity. In particular, an observed SE striking lineation of enhanced seismicity is shown to be a direct consequence of a deepening boundary between the crust and mantle SE of Parkfield, as evidenced by a deepening of the tremor and low-frequency earthquakes. Other evidence for a causal link between deep creep and off-fault seismicity is the observation that off-fault seismicity before and after the 2004 earthquake occurred in the same location. This is expected if the foreshocks are driven by an episode of deep creep and the aftershocks are driven by afterslip, both occurring on the same deep extension of the fault plane.

BIBLIOGRAPHY

Publications (in review)

Kim, A., D.S. Dreger, T. Taira, and R.M. Nadeau, Changes in repeating earthquake slip behavior following the 2004 Parkfield mainshock from waveform empirical Green's functions finite-source inversion, JGR-Solid Earth, (accepted, 2016).

Sammis, C.G., S.W. Smith, R.M. Nadeau and R. Lippoldt, Relating Transient Seismicity to Episodes of Deep Creep at Parkfield CA, Bull. Seismol. Soc. Am, (accepted, in revision), 2016.

REFERENCES

Aki, K., and P. G. Richards (1980), *Quantitative Seismology*, 2nd ed., Freeman and Co., New York.

Chen, K. H., R. Bürgmann, and R. M. Nadeau (2013), Do earthquakes talk to each other? Triggering and interaction of repeating sequences at Parkfield, Journal of Geophysical Research, 118, doi:10.1029/2012JB009486.

Chen, T. and N. Lapusta (2009), Scaling of small repeating earthquakes explained by interaction of seismic and aseismic slip in a rate and state fault model, J. Geophys. Res., 114, B01311, doi:10.1029/2008JB005749.

Dreger, D., R.M. Nadeau, and A. Chung, (2007), Repeating Earthquake Finite-Source Models: Strong Asperities Revealed on the San Andreas Fault, Geophys. Res. Lett., 34, L23302, doi:10.1029/2007GL031353.

Hanks, T. C., and W. H. Bakun (2008), M-log A observations of recent large earthquakes, *Bull. Seism. Soc. Am.,* 98,490, doi:10.1007/s00531-015-1217-8.

Johnson, K. M., D. R. Shelly, *and* A. M. Bradley *(*2013*),* Simulations of tremor-related creep reveal a weak crustal root of the San Andreas Fault*,* Geophys. Res. Lett.*,* 40*,* 1300–1305*, doi:*10.1002/grl.50216.

Johnson, L.R. and R.M. Nadeau (2002). Asperity model for an earthquake: static problem, *Bull. Seismol. Soc. Am.* **92** 672-686.

Johnson, L.R. and R.M. Nadeau, Asperity Model of an Earthquake - Static Problem, Bull. Seismol. Soc. Amer., 92, 672-686, 2002.

Johnson, L.R. and R.M. Nadeau, Asperity Model of an Earthquake: Dynamic Problem, Bull. Seismol. Soc. Am., 95, 75-108, 2005.

Johnson, L.R., An earthquake model with interacting asperities, Geophys. J. Int., 182, 1339-1373, doi: 10.1111/j.1365-246X.2010.04680.x, 2010.

Kim, A., D.S. Dreger, T. Taira, and R.M. Nadeau, Changes in repeating earthquake slip behavior following the 2004 Parkfield mainshock from waveform empirical Green's functions finite-source inversion, JGR-Solid Earth, (revised, resubmitted), 2016.

Mavrommatis, A.P., P. Segall, and K.M. Johnson (2014), A decadal-scale deformation transient prior to the 2011 Mw 9.0 Tohoku-oki earthquake, *Geophys. Res. Lett.*, *41,* 13, 4486-4494.

Nadeau, R.M. and L.R. Johnson (1998). Seismological studies at Parkfield VI: Moment release rates and estimates of source parameters for small repeating earthquakes, *Bull. Seismol. Soc. Am.* **88** 790-814.

Okada, Y. (1992), Internal deformation due to shear and tensile faults in a half space, *Bull. Seism. Soc. Am.*, *82*, 1018-1040.

Sammis, C.G., S.W. Smith, R.M. Nadeau and R. Lippoldt, Relating Transient Seismicity to Episodes of Deep Creep at Parkfield CA, Bull. Seismol. Soc. Am, (accepted, in revision), 2016.

Thurber, Clifford, H. Zhang, F. Waldhauser, J. Hardebeck, A. Michael, and D. Eberhart-Phillips (2006), Three-dimensional compressional wavespeed model, earthquake relocations, and focal mechanisms for the Parkfield, California, region." *Bull. Seism. Soc. Am.,* 96.4B, S38–S49.